MECHANIKA TEORETYCZNA
I STOSOWANA
Journal of Theoretical
and Applied Mechanics
3, 31, 1993

NEW TRENDS IN OPTICAL METHODS FOR EXPERIMENTAL MECHANICS. Part II: HIGH SENSITIVITY GRATING INTERFEROMETRY FOR IN-PLANE DISPLACEMENT MEASUREMENT

KRZYSZTOF PATORSKI

MAŁGORZATA KUJAWIŃSKA

Faculty of Fine Mechanics

Warsaw University of Technology

Recent developments in the high sensitivity grating interferometry for submicron in-plane displacement studies aiming at the automation of the data reduction process are presented. The implementation of phase methods of interferogram analysis using the polarized light approach together with the spatial carrier method are described. The versality, speed and accuracy of the methods and instrumentation developed are illustrated by the results of recent applications in plastic-elastic range of mechanics, fracture mechanics and studies of composite materials.

1. Introduction

The conventional moire method for studying in-plane displacements of the objects under load (Theocaris, 1969; Durelli and Parks, 1970) displays sensitivity limitations caused by technological difficulties with copying amplitude type binary diffraction gratings and a rapid decrease of the moire fringe contrast due to a finite gap between two superimposed structures. The upper frequency of the gratings to be copied is assumed to be 50 lines/mm what corresponds to the method basic sensitivity of 20 μm per fringe order. This sensitivity value is highly insufficient to conduct various investigations within the elastic deformation region.

In general, when higher sensitivity is needed it is necessary to switch to coherent illumination of the gratings and interferometry methods. The information on the departure of grating lines from straightness is coded in the departure of wave fronts of grating diffraction orders from the plane wave front. The sensitivity is directly proportional to the number of the diffraction order used. The deformed wave front can be compared with a plane reference wave front or, even better,

with its longitudinally reversed counterpart (frequently called as the conjugate wave front). In the latter case the sensitivity is doubled. High diffraction orders of the same number and opposite sign can be brought into interference by using symmetrical double beam illumination. This approach was used in the first studies on sensitivity increase of the moire method by Post (1971) and Matsumoto and Takashima (1973).

The so-called moire interferometry method (cf Post, 1987; Czarnek, 1991) represents an excellent improvement of the approach of using higher order mutually conjugate diffraction orders. It employs high frequency reflection type phase grating fixed to the plane surface of the object under load. It is a relatively new method, developed largely in the eighties. It matured quickly and due to its excellent characteristics like real-time whole field mapping, submicron sensitivity, high interference contrast, wide strain range, and easy alignment and operation, respectively, it is used in several laboratories for complete strain analysis in the elastic and plastic region including the residual strain analysis. The method is used for material behaviour studies – it suits ideally to investigation of composite materials in both the macro and micro-mechanics domains. Other exemplary applications include fracture mechanics, studies of joints of various types and verification of engineering designs by supplementing the method of finite element analysis.

Since in authors' opinion the name "moire interferometry" is a misleading one (there is no moire effect involved, two-beam interference only is encountered) and was given prematurely, in the following the name (high sensitivity) grating interferometry will be used. After a short review of the fundamentals and practice of the method some recent activities of the authors' research group are presented. They include studies of composite materials, residual stresses and fracture mechanics. The developments in optical and video processing methods of fringe patterns will be described as well. In particular the implementation of the phase methods for computer aided automatic interferogram analysis, i.e., temporal, spatial and carrier frequency phase stepping methods makes the grating interferometry technique an expected tool for laboratory and off-laboratory tests of materials, construction elements and solving various mechanical problems. The resulting increase in the measurement speed, accuracy, versatility and ease of application strengthens the position of the grating interferometry method among other experimental mechanics methods.

2. Principles

The principle of high sensitivity grating interferometry is shown schematically in Fig.1. Two mutually coherent illuminating beams A and B impinge on the reflection type specimen grating SG at the angles tuned to the first and minus

first diffraction order angle of SG. The $+1$ diffraction order of A and the -1 order of B propagate co-axially along the grating normal. Their wave fronts W_A and W_B are no longer plane.

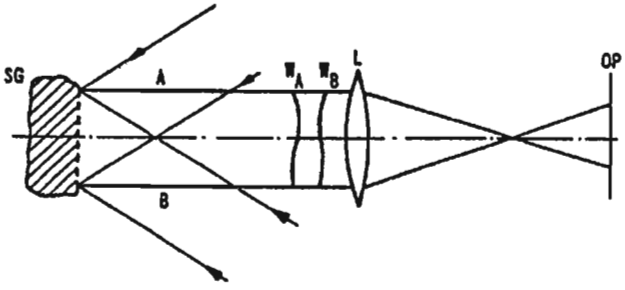

Fig. 1. Schematic representation of a double illuminating beam grating interferometry for in-plane displacement studies. SG – specimen grating; L – imaging optics; OP – observation plane; W_A, W_B – wavefronts of +1 and -1 diffraction orders

The amplitudes in the observation plane OP conjugate to SG can be described as

$$E^A_{+1}(x,y) = \exp\Big\{\mathrm{i}\Big[\frac{2\pi}{d}u(x,y) + \frac{2\pi}{\lambda}w(x,y)\Big]\Big\} \tag{2.1}$$

$$E^B_{-1}(x,y) = \exp\Big\{-\mathrm{i}\Big[\frac{2\pi}{d}u(x,y) - \frac{2\pi}{\lambda}w(x,y)\Big]\Big\} \tag{2.2}$$

where d is the spatial period of the specimen grating whose lines are perpendicular to the x axis (lying in the figure plane), $u(x,y)$ is the in-plane displacement function corresponding to the departure of the grating lines from straightness, $w(x,y)$ is the out-of-plane displacement function corresponding to the deformation of the specimen surface under load. For simplicity, the amplitude of the diffraction orders has been normalized to unity.

It can be seen that wave front deformations caused by in-plane displacements are equal in both diffraction orders but longitudinally reversed. On the other hand, the wave front deformations due to out-of-plane displacements have the same value and sign in both interfering beams. Therefore the influence of out-of-plane displacements is eliminated by the interference. Thus assuming that out-of-plane displacements give only small variations in slope of the wave fronts (the departure from this condition was theoretically investigated by McKelvie and Patorski, 1988), the intensity distribution of the interferogram becomes

$$\Big|E^A_{+1} + E^B_{-1}\Big|^2 = 2\Big[1 + \cos\big(\frac{4\pi}{d}\big)u(x,y)\Big] \tag{2.3}$$

The fringes observed in the interferometer represent a contour map of in-plane displacements with half a period sensitivity. For example, when using the specimen

grating of spatial frequency 1200 lines/mm the basic sensitivity is 0.47 μm per fringe order.

When the double beam illumination system is angularly misaligned, the carrier fringes are introduced into the interferogram. The last equation transforms into

$$I(x,y) = 2\Big\{1 + \cos\Big[2k\theta_x + \frac{4\pi}{d}u(x,y)\Big]\Big\} \tag{2.4}$$

where θ_x designates the angle between the diffracted orders and the grating normal, $k = 2\pi/\lambda$.

The ease in introducing dense carrier fringes into the interferogram facilitates the use of the moire fringe technique for processing the interferograms. For example, the subtraction of the interferometer and grating errors at the initial no load stage, the comparison between two load levels and the subtraction of the uniform part of a displacement field can be performed. Two interferograms with carrier fringes are recorded for the two stages to be compared. Their superimposition results in moire fringes which map the difference in in-plane displacements between the two stages of the object. More sophisticated applications include measuring of out-of-plane displacements (Basehore and Post, 1982; Patorski, 1986), real time differentiation of in-plane displacement patterns (Patorski et al., 1987; Patorski and Wojciechowska 1990) and shear strain determination (Patorski, 1988). As will be shown in the following, the ease in introducing carrier fringes will be exploited in the carrier frequency phase stepping method used for automatic fringe pattern analysis.

To obtain a complete strain information a crossline specimen grating is commonly used. It is usually produced by a replication process, i.e., casting a thin layer of, for example, epoxy resin on the specimen surface by a special mold (see, for example, Post (1987) or Walker (1988)). A crossline grating requires two pairs of illuminating beams for its readout. A simple and convenient way for doing it will be described in the following Section together with recent improvements aiming at the development of the system for automatic data processing.

3. Implementation

Among various interferometer designs used to measure two orthogonal in-plane displacement fields two configurations deserve particular attention. These are the interferometer with three illumination beams developed at Strathclyde University, Glasgow (Walker, 1988) and four-beam interferometer developed at Virginia Polytechnic Institute and State University (Czarnek, 1991). In authors' research group the latter version was adopted and then modified to enable automatic interfero-

gram reduction process. Figure 2 shows a schematic representation of the basic configuration.

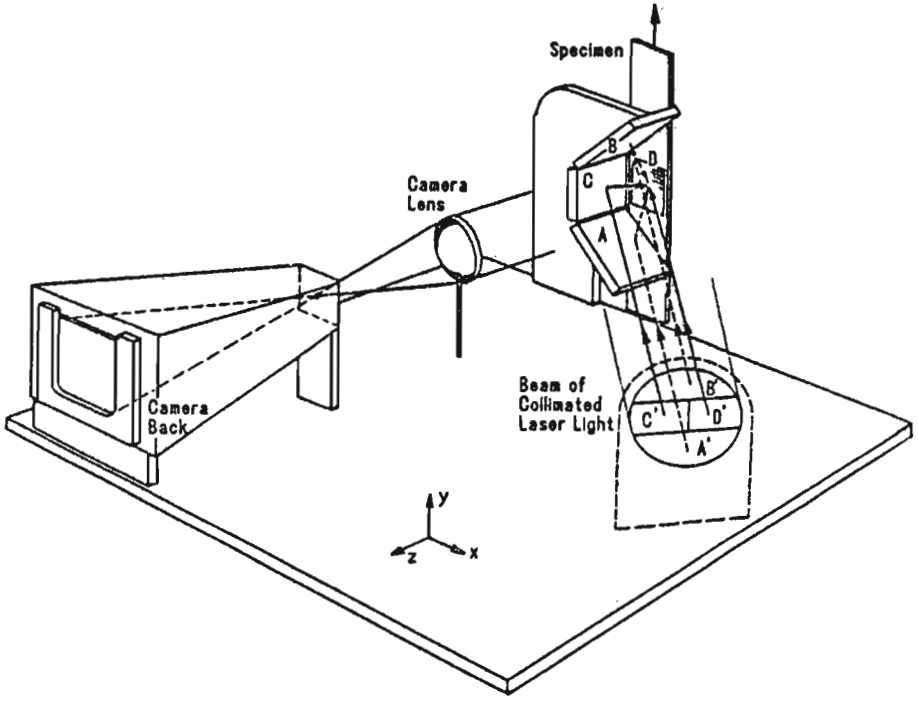

Fig. 2. Schematic drawing of a compact four-beam grating interferometer

The illuminating beams are obtained from an expanded laser beam by using three mirrors A, B, and C fixed directly on the sample under test with a cross line specimen grating. The grating frequency is 1200 lines/mm. The fragments C' and D' of the collimated beam illuminate the vertical lines of the specimen grating and generate the interferogram corresponding to the map of displacements $u(x, y)$. The fragments A' and B' impinge first on the mirrors A and B positioned at 45 deg to the plane xz and perpendicular to the specimen surface. The beams A' and B' generate the interference fringes which constitute the map of displacements $v(x, y)$.

Since the illuminating system and the element under test are bound together the influence of external vibrations on the interferogram is considerably reduced. The additional property worth mentioning is that any rigid body rotation introduced during deformation is equally represented in the two patterns. In consequence the shear strain can be calculated from the patterns without error. That is, all three strain tensor components can be measured. The three-mirror interferometer

head designed and manufactured at the Institute of Design of Precise and Optical Instruments is shown in Fig.3.

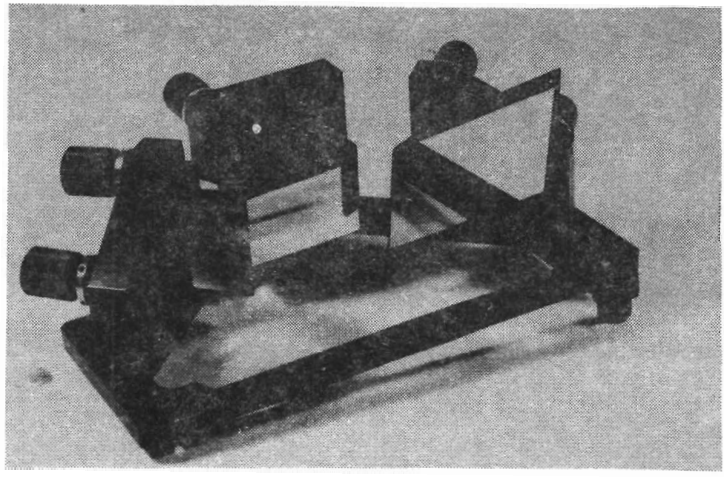

.Fig. 3. The head of three-mirror grating interferometer

Although the grating interferometry method is mainly destined for the measurement of in-plane displacements there exist cases in which the out-of-plane deformation information is required as well. For this purpose the configuration shown in Fig.2 is readily modified by adding a reference beam using a beam splitter PS, and a reference plane mirror, MR, see the combined configuration on Fig.5 (Sałbut, 1993).

To facilitate the automatic computer-aided analysis of interference fringes the implementations of the phase shifting technique have been proposed (Salbut and Patorski, 1990; Kujawińska et al., 1991; Sałbut et al., 1992) including both temporal and spatial approaches. The polarized light approach was selected because of the common path propagation of the two interfering beams.

Figure 4 shows the basic configuration implementing the phase-shifting technique. Specimen grating SG is illuminated by two beams with orthogonal polarization. Since SG is alluminium coated it influences the state of polarization of diffracted beams; compensators C are used to deal with this problem. The diffracted beams can be circularly or linearly polarized. Their interference is facilitated by analyzer A.

For example, in the case of orthogonal circular polarization of the diffraction orders their amplitudes can be written as

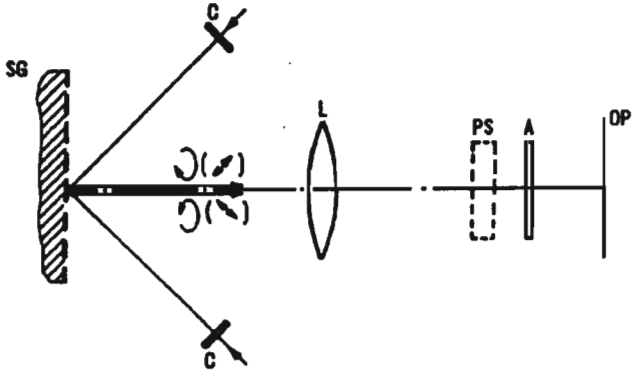

Fig. 4. Schematic representation of the polarization phase shifting grating interferometry. C – polarization compensator; A – analyzer; PS – phase-shifter for the case of linearly polarized light only; SG – specimen grating; L – imaging optics; OP – observation plane

$$\mathbf{E}_{+1} = \begin{bmatrix} 1 \\ \mathrm{i} \end{bmatrix} a \exp\left\{\mathrm{i}\left[\frac{2\pi}{d}u(x,y) + \frac{2\pi}{\lambda}w(x,y)\right]\right\} \tag{3.1}$$

$$\mathbf{E}_{-1} = \begin{bmatrix} 1 \\ -\mathrm{i} \end{bmatrix} a \exp\left\{-\mathrm{i}\left[\frac{2\pi}{d}u(x,y) - \frac{2\pi}{\lambda}w(x,y)\right]\right\} \tag{3.2}$$

where the subscripts of $\mathbf{E}$ designate the diffraction order number, a is the amplitude coefficient, other denotations remain the same. The Jones matrixes

$$\begin{bmatrix} 1 \\ -\mathrm{i} \end{bmatrix} \qquad \text{and} \qquad \begin{bmatrix} 1 \\ \mathrm{i} \end{bmatrix}$$

relate to right and left circular polarizations, respectively. After passing through the analyzer the beam amplitudes become

$$\mathbf{E}^{A}_{+1} = \mathbf{M}_A \mathbf{E}_{+1} \tag{3.3}$$

$$\mathbf{E}^{A}_{-1} = \mathbf{M}_A \mathbf{E}_{-1} \tag{3.4}$$

where

$$\mathbf{M}_A = \begin{bmatrix} \cos^2\alpha & \cos\alpha\sin\alpha \\ \cos\alpha\sin\alpha & \cos^2\alpha \end{bmatrix}$$

is the Jones matrix of the analyzer. After calculations, the intensity distribution in the observation plane is

$$I(x,y) = 2a^2\left\{1 + \cos\left[\frac{4\pi}{d}u(x,y) + 2\alpha\right]\right\} \tag{3.5}$$

By rotating the analyzer by angle α a phase shift of 2α is realized.

In the second case with diffracted beams of orthogonal linear polarization the phase shifting can be realized by phase shifter PS, see Fig.4, of the form

1. Rotational polarizer, as described above, placed behind the $\lambda/4$ plate oriented at 45 deg to the polarization planes of the diffraction orders.

2. Several phase plates, the number of which is related to the number of interferograms required by the phase stepping algorithm used.

3. A laterally translated Wollaston prism or other polarization compensator that shifts the phase between perpendicularly polarized diffraction orders.

Figure 5 shows the implementation of the phase shifting method described above for measuring the two orthogonal in-plane displacement fields (path I) as well as the out-of-plane displacement (path II). In the case of the u displacement field (along the x direction) opposite directions of polarizations are due to the different number of reflections on the way of two superimposed diffraction orders (the phase of the electric vector component perpendicular to the incidence plane is shifted by π).

In the case of measuring the v displacement field (along the y direction) the number of reflections is the same for both parts A' and B' of the illuminating beam so the direction of polarization in one illuminating beam should be changed by the half-wave plate $H1$. Similar situation occurs for w-displacement. In order to supply the orthogonal polarized beams from the Twyman-Green interferometer configuration used for specimen shape measurement the additional quarter wave-plate is inserted in front of mirror MR. This configuration enables alternative measurements of u, v and w displacements by the phase-shifting method, while the proper parts of beam are cut off and the phase shift is performed by the rotating analyser.

The configuration shown in Fig.5 is used for the so-called temporal phase shifting for the computer aided analysis of the interferogram data. As explained in the first part of the paper, this approach requires recording sequentially in time three, four, or five interferograms mutually shifted in phase. For example, when using the five step technique, which provides a self-calibrating procedure for linear errors of phase steps, the value of the in-plane displacement function $u(x,y)$ is calculated as

$$u(x,y) = \frac{d}{4\pi} \arctan \frac{2(I_2 - I_4)}{I_1 - 2I_3 + I_5} \tag{3.6}$$

where I_i are the intensity values in a given pixel obtained for the phase-shifted fringe patterns, $\delta_i = 2\alpha$.

Since any random phase changes occurring in the course of taking three, four or five recordings are prohibited, only static events can be studied by the temporal

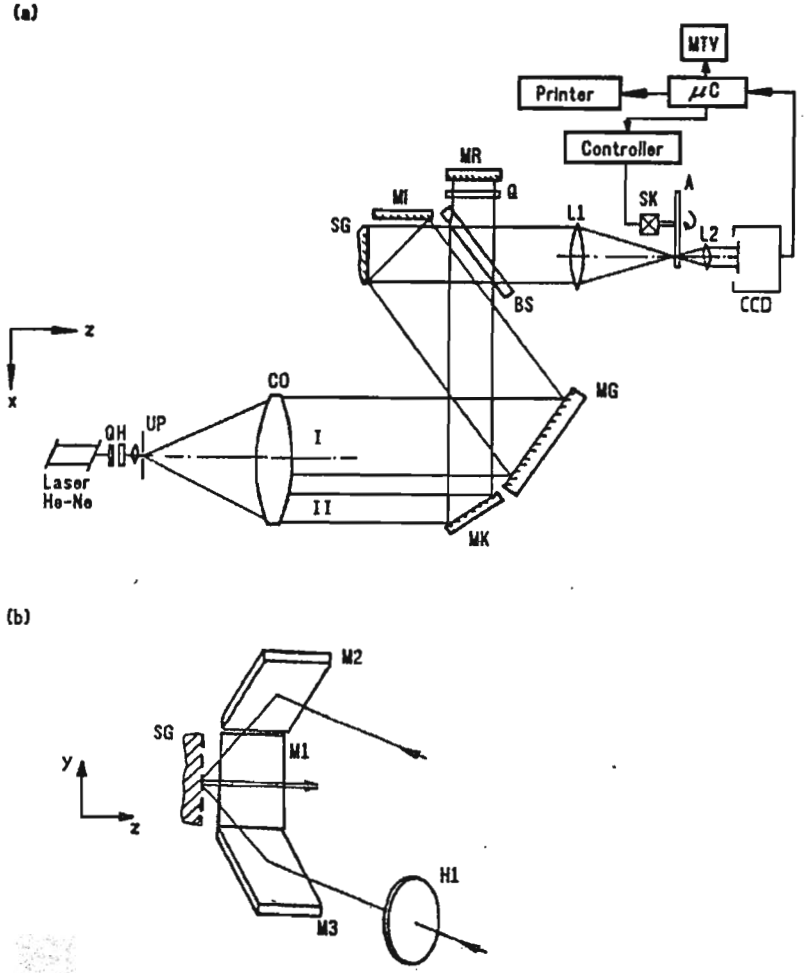

Fig. 5. Polarized light phase shifting combined grating/Twyman-Green interferometer in the xz cross section (a) and in the yz cross section (b). UP – pinhole; CO – collimator objective; Q and H – quarter- and half-wave plates of the compensator; MG and MK – mirrors directing beams into interferometers; BS – beamsplitter; MR – reference mirror in Twyman-Green interferometer; $L1$ and $L2$ – imaging optics; $M1$, $M2$, $M3$ – grating interferometer mirrors; SG – specimen grating; A – rotating analyser; SK – step motor

approach. The spatial phase shifting version developed in the authors' laboratory removes this limitation. It is shown schematically in Fig.6.

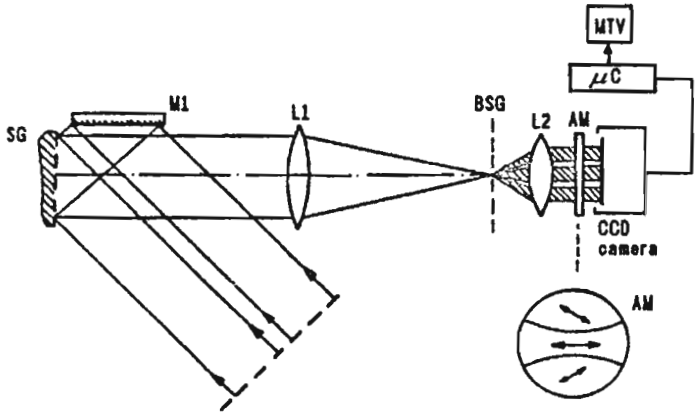

Fig. 6. Three-channel polarization grating interferometry. *BSG* – beams splitter grating; *AM* – analyzer modulus; other symbols as in previous figures

A triple interferogram replication at the output plane is obtained by inserting a sinusoidal transmittance diffraction grating *BSG* near the focus of objective *O*1. Spatial separation of the three images is done by proper selection of the frequency of *BSG*. The required phase shifts are introduced by three properly oriented analyzers (modulus *AM*). Either a beam splitter grating should have equal diffraction efficiencies in the orders -1, 0, and $+1$ or the normalization of the intensities of side images with respect to a central one is required. Correspondingly, the function $u(x, y)$ is calculated from the formula

$$u(x,y) = \frac{d}{4\pi} \arctan \frac{I_0 - I_{-1}}{I_{-1} + I_{+1}} \tag{3.7}$$

The possibility of working at a one-frame rate in the spatial phase shifting configuration must be paid for. The accuracy obtained is usually lower than that for the temporal approach.

Finally, the realization of the spatial carrier phase shifting (*SCPS*) approach should be commented upon. As it was shown in first part of this paper, the *SCPS* method combines the advantages of a single interferogram analysis connected with the Fourier Transform method with the simplicity and robustness of the *PS* approach. The basic requirement for this method is to introduce the proper carrier frequency f_0, such that the basic intensity equation is given as

$$I_i(x,y) = 2a^2\left\{1 + \cos\left[\frac{4\pi}{d}u(x,y) + 2\pi f_0\left(x + \frac{i}{4f_0}\right)\right]\right\} \tag{3.8}$$

where $i = 1, ..., 5$.

In practice it means that the number of reference fringes while using the sampling frequency $N = 128$ equals 32 (for $N = 256$, $64 \rightarrow$ fringes). It can be easily achieved (for measurement of u and v displacements) by the rotation of one of the interferometer mirrors under zero loading condition (homogeneous interferometric field) or by changing the direction of the beam illuminating the interferometer introduced by the rotation of the mirror MG or the lateral displacement of the collimating objective CO. Additionally the lateral displacement of CO being measured can be applied to controlled monitoring of the homogeneous displacement and adaptive changes of the carrier frequency to fulfill the requirements of the method (Han and Post, 1989)

The carrier frequency required for out-of-plane displacement is introduced by rotation of the mirror MR in the Twyman-Green interferometer.

The displacement maps are calculated according to Eq (3.6) in which the intensities I_i refer to intensities in the sequential pixels.

The $SCPS$ method enables monitoring of the displacement and strain fields for dynamic processes (e.g., crack propagation) and in an unstable environment. Future works will lead to opto-mechanical configuration which enables simultaneous measurement of u and v displacements.

A short discussion of the accuracy of the phase shifting method was already given in the first part of the paper. It is mainly influenced by the departure of fringe intensity profile from a sinusoidal one, the changes in the background and contrast functions of the interferogram during the measurement, and the difference between the phase shifts in the component images.

The main sources of errors in the polarization method are as follows

1. the changes in the mean intensity, contrast, and phase shift of the succeeding interferograms caused by noncircular/nonlinear polarization of the interfering diffraction orders,

2. incorrect analyzer rotation,

3. the detector nonlinearity causing nonsinusoidal fringe profile,

4. incorrect phase shifts caused by the vibrations and environmental instabilities during the measurement.

A comparative error analysis for the temporal and spatial approaches is given in detail in the works by Kujawińska et al. (1991) and Salbut et al. (1992). In short, the temporal approach gives better resolution and accuracy, and the multichannel method, although providing the possibility for testing time dependent events, lacks some of the advantages of the conventional sequential phase stepping. Moreover high quality imaging optics and low noise detectors should be used.

The errors of the in-plane displacement measurement have periodic distribution with the frequency equal to (or double) that of the fringe patterns. When the frequency of interferogram fringes is high the errors change quickly, leading to large errors in the strains calculated as the derivatives of in-plane displacement fields.

As for the carrier frequency phase shifting method the main sources of errors and their character remain the same although we refer to spatial but temporal variations in the background and fringe contrast functions. Also here as in all spatial techniques the requirements for the quality of the detector are higher than in the temporal techniques.

4. Experimental works

The arrangement shown in Fig.5 was used for the experimental verification of polarization PS and $SCPS$ methods of fringe pattern analysis for measuring u and v in-plane displacements and strain analysis. One of the first experiments aiming at the experimental verification of a strict analytical solution was performed using an aluminium tensile specimen with a central hole. Figure 7 shows the interferograms obtained in x and y directions and the results of analysis (by TPS) in the form of 3-D plots of u and v fields of in-plane displacement. The strains were calculated as

$$\varepsilon_x = \frac{\delta u(x,y)}{\delta x} \qquad \varepsilon_y = \frac{\delta v(x,y)}{\delta y}$$
$$\gamma_{xy} = \frac{\delta u(x,y)}{\delta y} + \frac{\delta v(x,y)}{\delta x} \tag{4.1}$$

The experimental results of strains ε_x, ε_y and γ_{xy} (without any filtration operations performed) are shown in Fig.8a÷c. Figures 8d÷f present the respective theoretical strain distributions. The experiment shows good agreement between the experimental and theoretical strain distributions. In order to avoid the big peak-to-valley errors obtained in the large strain concentrations regions (the hole edge) the special attention has to be paid to the grating replication process at the edge of the object.

The combined interferometer system for u, v and w displacement measurements (Fig.5) was applied to test the area around a crack tip in a tensile steel sample. Figure 9 shows the fringe patterns with a proper carrier frequency for $SCPS$ method and the results of the analysis of in-plane u and v displacement and the shape of the specimen under the load of 10000N in the form of contour maps (Fig.9d÷f) and 3-D maps (Fig.9g÷i). The specimen was loaded above the

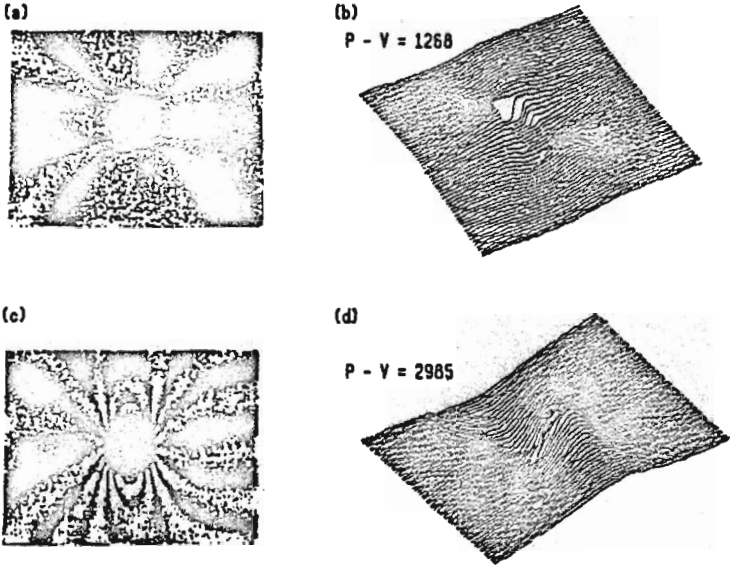

Fig. 7. Experimental results for u and v in-plane displacements measurements for tensile aluminum specimen: (a) and (c) interferograms; (b) and (d) 3-D plots of displacement fields, respectively

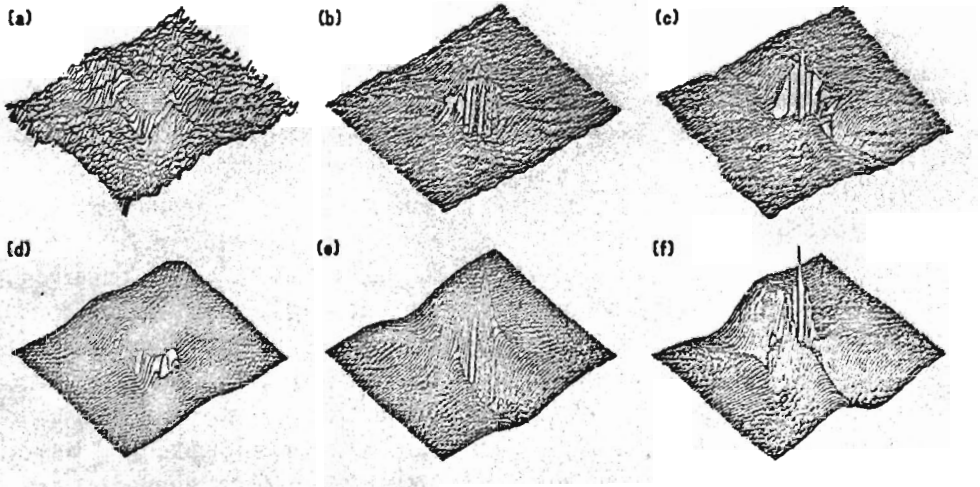

Fig. 8. Experimental results of strain calculation: (a) – ε_x, (b) – ε_y, (c) – γ_{xy}. Theoretical strain distributions: (d) – ε_{xt}, (e) – ε_{yt}, (f) – γ_{xyt}

plasticity limit ($F = 20$ kN) and then the load was decreased to 2 kN. The differential displacement maps $u_{20} - u_2$ and $v_{20} - v_2$ were calculated (Fig.10b and c). The region under analysis covers a part of a notch filled with resin (area A shown in Fig.10a and b) and it does not contain the proper information. The differential displacements were used for strain map calculation (Fig.10d÷f). The results support the theoretical considerations on the description of the plasticity region distribution around the crack tip.

Several experiments were performed for the composite material testing, aiming at local and global material constant description (Jancelewicz et al., 1993), detection of material defects (Poon et al., 1993) and cracks detection and monitoring (Kujawińska, 1992).

As an example, the measurements of two composite (carbon fibre/epoxy) specimens with the ply-drop-offs are presented (Poon et al., 1993). Specimen A consists of two layers of woven material on each side (with orientation $(45°, -45°)$ and $(-45°, 45°)$) and 2 plies of unidirectional laminate in which each ply has five laminae with orientation of $90°/90°/0°/90°/90°$. One ply terminates in the middle as shown in Fig.11a to form a tapered panel. Specimen B consists of 3 layers of UD tape on each side with the orientation $0°$. The core combines 4 plies of UD laminate. Each ply has five laminae at the orientation of $90°/90°/0°/90°/90°$. One ply is cut into two and stacked as shown in Fig.12a to form a flat panel with two ply drop-offs. Composite specimens are loaded in a 4 point bending rig such that the specimen 11a and 12a is subjected to a longitudinal tensile strain on the right and a compressive strain on the left. The specimen grating is attached to the central region where it exposed to a pure bending.

Figures 11b and 11c show the u and v displacement patterns at a bending moment 0.38 Nm. The 3-D maps of the respective displacements, obtained by TPS method are shown in Fig.11d and e. From Eq (4.1), the strains ε_x, ε_y and γ_{xy} are calculated and shown in Fig.11f÷h. For homogeneous isotropic material under a constant bending moment, the strain ε_y varies linearly in the x direction and the strain γ_{xy} is zero. However Fig.11f÷h shows that ε_y varies linearly in the middle region only and γ_{xy} varies by a significant magnitude of the order ε_y. The existence of non-zero ε_x and γ_{xy} is expected for composites where different materials interact with each other and redistribute their strains and stresses to reach the state of equilibrium. For this specimen the ε_x reach its maximum near the interface of UD/woven where the regions are under longitudinal tensile load and minimum near the interface of UD/woven where the regions are under longitudal compressive loading. In the study of the failure process, it is of interest to know whether it fails by desalination at UD/woven interface due to ε_x or at woven/woven interface due to γ_{xy} or by matrix cracking or fibre breakage due to ε_y or fails by the combination of the states of strain. The mode of failure of course depends on how fast these strains reach their critical values. It means that the

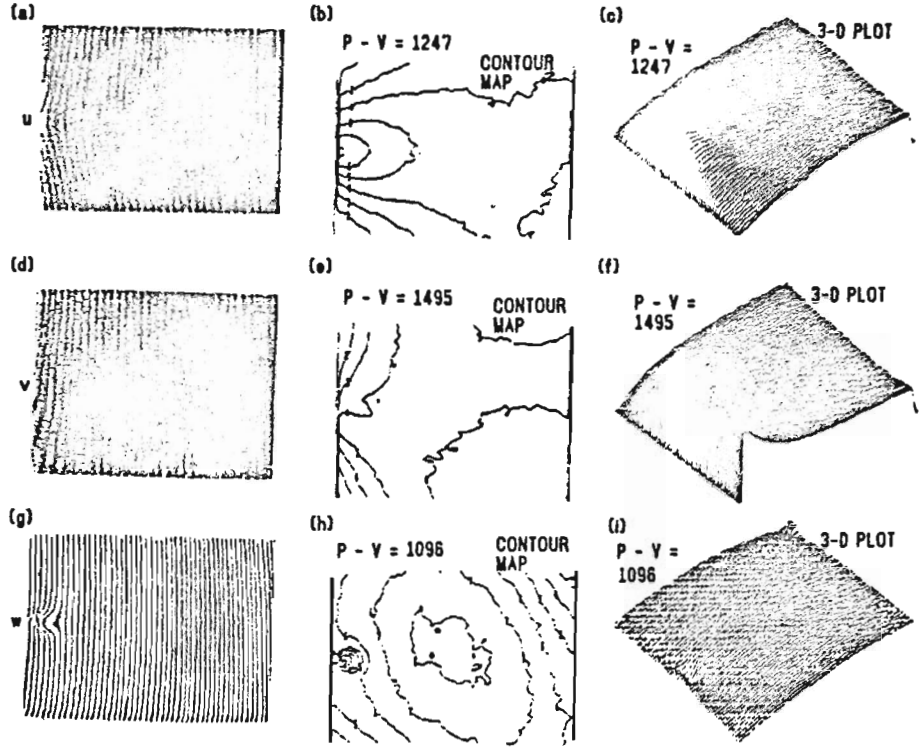

Fig. 9. The u, v and w displacement measurement around a crack tip at the steel specimen under tensile load $F = 10000$ N, (a-c) – interferograms, (d-f) – the contour maps and (d-i) – 3-D maps for u, v and w respectively

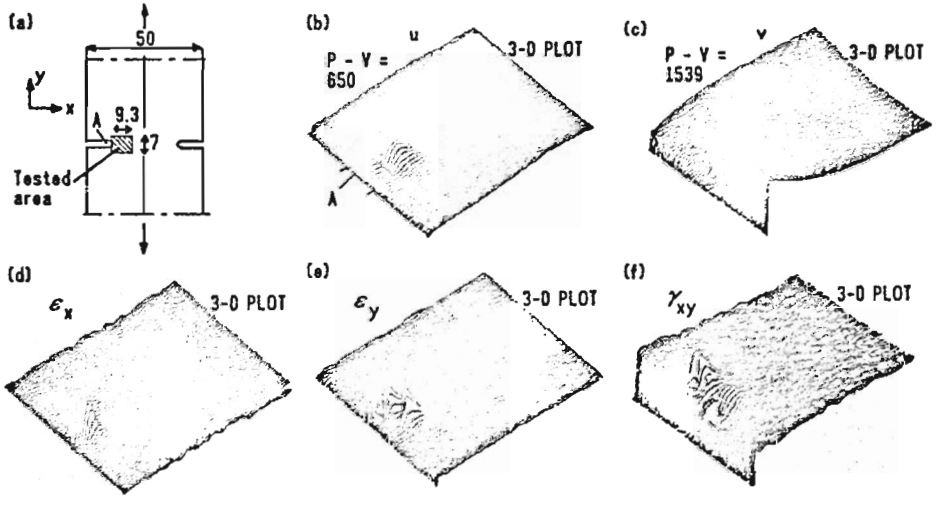

Fig. 10. The displacement and strain distributions around the crack tip loaded above the plasticity limit; (a) – the specimen configuration, (b) and (c) – 3-D plots of u and v displacement map; strain distributions: (d) – ε_x, (e) – ε_y and (f) – γ_{xy}

mode of failure can be assessed by the ratio between the strain values and their critical values.

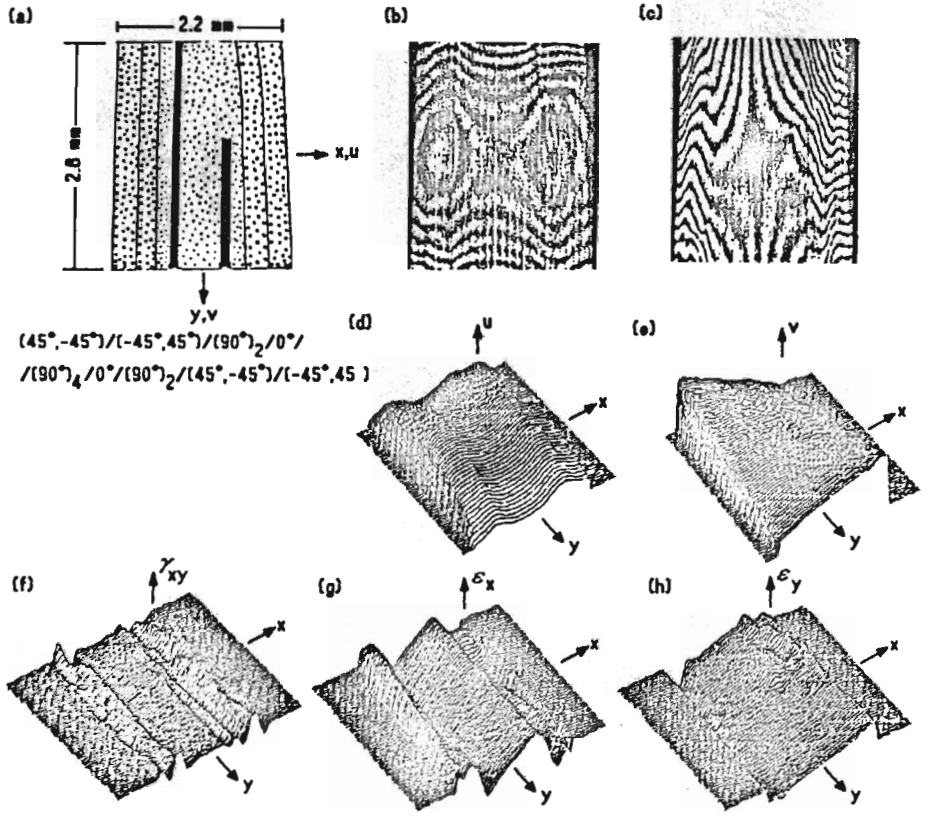

Fig. 11. The composite carbon fibre/epoxy specimen A under 4 point bending. (a) – laminate lay-up geometry; (b), (c) – interferograms for u and v displacement fields; (d), (e) – their calculated 3-D plots, respectively. The strain distributions (f) – γ_{xy}, (g) – ε_x and (h) – ε_y

Figure 12 shows the u and v displacement patterns of the specimen B before and after a crack is formed at the ply drop-off for the same bending moment 1.35 Nm. As in specimen A, strain concentration ε_y arises, as indicated in Fig.13b at the ply drop-off. For further loading, a crack forms at the ply drop-off as shown in Fig.7d and e. The strain maps before and after crack, respectively for the same load, are plotted in the same scale in Fig.13. After the crack is formed, the load released by the crack will transfer to neighboring regions and redistribute the state of strain which results in strain concentration of ε_x, ε_y and γ_{xy} around the crack. All the strains are higher after the crack than before the crack was formed. It indicates that some forms of plastic deformations took place when a crack was

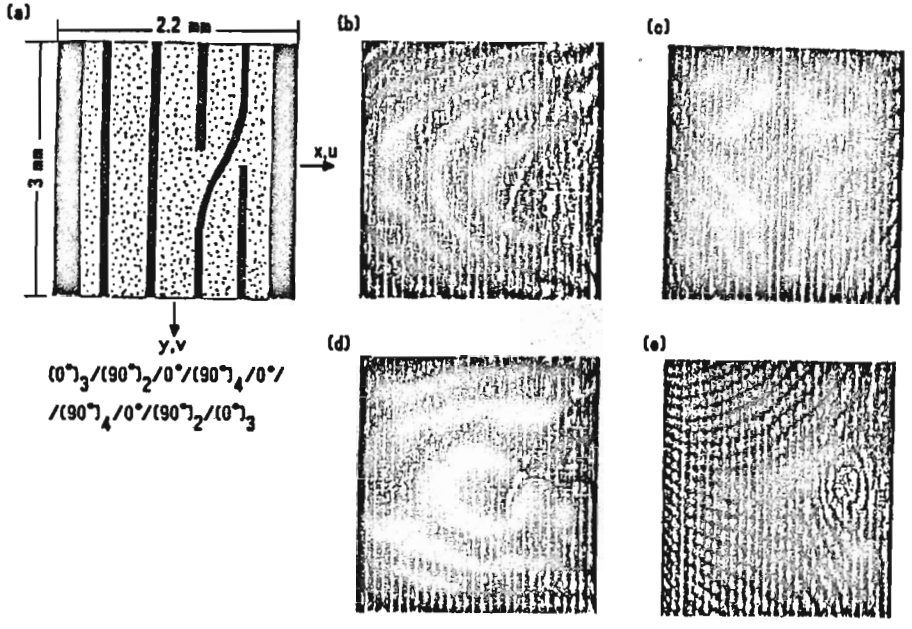

Fig. 12. The composite carbon fibre/epoxy specimen B under 4 point bending. (a) – laminate lay-up geometry; (b), (c) – interferograms for u and v displacement fields and (d), (e) – interferograms for u and v displacement after crack

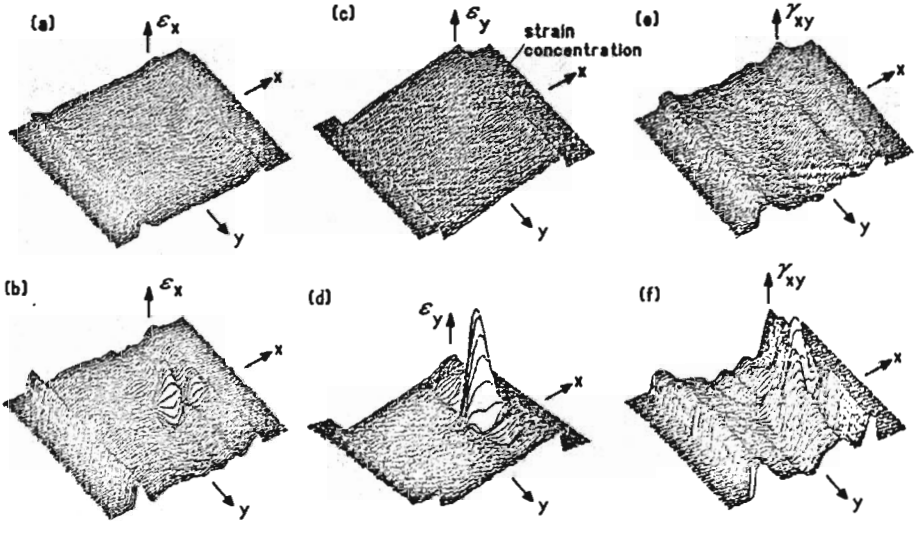

Fig. 13. Comparison of strains after a crack is formed at the ply drop-off. ε_x map (a) before and (b) after crack. ε_y (c) before and (d) after crack. γ_{xy} (e) before and (f) after crack

formed at the ply drop-off. Away from the crack, the difference between the strain before and after the crack represents the residual strain in the specimen.

5. Conclusions

Grating interferometry combined with an automated fringe pattern analysis method and several modifications of opto-mechanical system provides a robust and highly efficient method for measuring strain fields in various types of materials, in particular composites which are difficult to model in terms of strength and failure mechanisms. Grating interferometry allows global and local approach to strain and material constant measurement. Remarkable results concerning plasticity regions and various joints investigations, local strain distribution, crack initiation, re-distribution of strains after crack, residual strain investigation in both conventional and new technological materials including wide range of composite materials, smart structures etc. are reported.

The capabilities of the method and the advantages of the automatic fringe pattern analysis enable full implementation of hybrid methods of deformation and strain analysis combining the experimental technique with the finite element techniques.

It has been shown in Part I and Part II of this paper that the recent developments in optical methods for experimental mechanics aiming at the automation of data processing provide not only powerful means for less time-consuming and more accuracy reliable experiment, but also a powerful tool for CAD (e.g. moire topography) and FEM (grating interferometry) methods.

Acknowledgment

The authors are grateful to Mr L.Salbut for his help in experimental work and fruitful discussions regarding various applications of the system. The authors gratefully acknowledge the support of the Committee of Scientific Research within the research project PB 0618/S2/92/03.

References

1. BASEHORE M.L., POST D., 1982, *Displacement fields (U,W) obtained simultaneously by moire interferometry*, Appl.Opt., 21, 2558-2562

2. CZARNEK R., 1991, *Three mirror, four-beam moire interferometer and its capabilities*, Opt.Lasers Eng., 15, 93-101

3. HAN B., POST D.,1989, *The tilted-plate method for introducing carrier fringes of extension in moire interferometry*, Exp.Tech., July, 25-29

4. JANCELEWICZ B., SALBUT L., KUJAWIŃSKA M, 1993, *Application of grating interferometry for global and local measurements of in-plane displacement and strain in multilayer composite structures*, J.Theor.Exp.Mech., submitted for publication

5. KUJAWIŃSKA M., 1992, INTERNAL IKPPiO REPORT *Investigation of composite material testing by moire interferometry method*, Warsaw Univ. of Techn., IKPPiO

6. KUJAWIŃSKA M., SALBUT L., PATORSKI K., 1991, *Three-channel phase stepped system for moire interferometry*, Appl.Opt., **30**, 1633-1635

7. KUJAWIŃSKA M., PATORSKI K., 1993, *New trends in optical methods for exzperimental mechanics. Part 1: Moire and grating projection techniques for shape and deformation measurement*, Mech.Teoret.i Stos., **31**, 3

8. KUJAWIŃSKA M., WÓJCIAK J., 1991, *Spatial phase-shifting techniques of fringe pattern analysis in experimental mechanics*, Proc. SPIE, **1554B**, 325-329

9. MATSUMOTO K., TAKASHIMA M., 1973, *Improvement on moire technique for in-plane deformation measurements*, Appl.Opt., **12**, 858-864

10. MCKELVIE J., PATORSKI K., *Influence of the slopes of the specimen grating surface on out-off-plane displacements measured by moire interferometry*, Appl.Opt., **27**, 4603-4605

11. PATORSKI K., 1986, *A method for obtaining out-of-plane displacements by moire interferometry*, Opt.Commun., **60**, 128-132

12. PATORSKI K., 1988, *Shearing interferometry and the moire method for shear strain determination*, Appl.Opt., **27**, 3567-3572

13. PATORSKI K., POST D., CZARNEK R., GUO I., 1987, *Real-time optical differentation for moire interferometry*, Appl.Opt., **26**, 1977-1982

14. PATORSKI K., WOJCIECHOWSKA M., 1990, *Real-time differentiation of moire interferometry patterns by incoherent superimposition of lateral shear interferograms*, Opt.Appl., **20**, 93-100

15. POST D., 1987, *Moire interferometry*, in *SEM Handbook of Experimental Mechanics*, Kobayashi A.S., Ed., Prentice Hall, Englewood Cliffs

16. POON C.Y., KUJAWIŃSKA M., RUIZ C., 1993, *Strain measurement of composites using an automated moire interferometry method*, Measurement, in press

17. SALBUT L., PATORSKI K., 1990, *Polarization phase shifting method for moire interferometry and flatness testing*, Appl.Opt., **29**, 1471-1473

18. SALBUT L., PATORSKI K., KUJAWIŃSKA M., 1992, *Polarization approach to high-sensitivity moire interferometry*, Opt.Eng., **31**, 434-439

19. SALBUT L., 1993, *Automatic grating interferometer for composite material testing*, Conf.Proc. "Computer Aided Metrology", Zegrze, May 1993

20. WALKER C., 1988, *Moire interferometry for strain analysis*, Opt.Lasers Eng., **8**, 213-262

Nowe kierunki rozwoju optycznych metod mechaniki doświadczalnej. Część II: Interferometria siatkowa o wysokiej czułości do pomiaru przemieszczeń w płaszczyźnie

Streszczenie

Przedstawiono wyniki prac dotyczących automatyzacji procesu przetwarzania danych otrzymywanych w interferometrze siatkowym do badania submikronowych przemieszczeń w płaszczyźnie. Opisano realizację metody dyskretnej zmiany fazy analizy interferogramów z wykorzystaniem światła spolaryzowanego oraz częstości nośnej. Wszechstronność, szybkość i dokładność opracowanych metod i aparatury zilustrowano wynikami ostatnich prac doświadczalnych z zakresu mechaniki stanów plastyczno-sprężystych, mechaniki pękania i badań materiałów kompozytowych.

Manuscript received March 22, 1993; accepted for print March 31, 1993